The 2022 World Congress on
Advances in Civil, Environmental, & Materials Research (ACEM22)
16-19, August, 2022, GECE, Seoul, Korea

Simplified Mechanical Model for Regional Seismic Collapse Performance Prediction of RC Frame and URM Structures

Li-Ling Yu[1)], Zhi-Qian Dong[2)] and *Gang Li[3)]

[1), 2) 3)] *State Key Laboratory of Coastal and Offshore Engineering, Dalian University of Technology, Dalian, Liaoning Province 116024, China*
[3)] gli@dlut.edu.cn

ABSTRACT

Unreinforced masonry (URM) structures and reinforced concrete (RC) frame structures account a large proportion in low- and multi-story buildings. Previous earthquakes indicate that these structures have high seismic collapse fragility, resulting in huge economic losses and casualties. Reliable regional seismic collapse performance prediction of URM structures and RC frame structures contributes the scientific earthquake prevention of a region so as to effectively mitigate seismic disaster loss. The number of buildings included in a region may be excessive, which makes the regional seismic collapse performance prediction adopted the refined finite element models become extraordinarily inapplicable due to their complexity of modeling process, as well as the time-consuming and convergence difficulty during nonlinear analysis. In this study, the equivalent single-degree-of-freedom (ESDOF) model that represents the global mechanical behaviors during the collapse of RC frames and URM structures is developed based on the IK deterioration model that has relatively comprehensive consideration of deterioration behaviors. For simplifying the parameter determination procedure of the structural ESDOF model to well apply to the regional seismic collapse performance prediction, a simplified method that uses the structural component hysteretic model parameters to directly solve the structural ESDOF model parameters is proposed based on the rigid plane assumption of structural floor slab, basic theory of the nonlinear pushover analysis as well as the empirical models from experimental data for RC columns and URM walls. Take the pseudo-static collapse experiment of an RC frame as example, comparison with the experimental force-displacement response is conducted to demonstrate that the accuracy of the ESDOF model.

1. INTRODUCTION

Unreinforced masonry (URM) structures and RC frame structures are some of the

[1)] Ph.D. Candidate
[2)] Associate Professor
[3)] Professor

most common structural forms of low- and multi-story buildings in many countries (Wu 2009, Lu 2012, Quiroz 2014 and Dolatshahi 2014). Previous earthquake disasters (Swinbanks 1995, Otani 1999, Bothara 2010 and Sandoval 2021) indicate that these structures often experience severe damage and collapse when subjected to destructive earthquakes due to their high seismic vulnerability, resulting in huge economic losses and casualties. Therefore, the reliable regional seismic collapse performance prediction of URM structure and RC frame structure is necessary, which contributes the scientific earthquake prevention of a region so as to effectively mitigate seismic disaster loss.

The micro-scale refined finite element models (Chaimoon 2007 and Shakarami 2018) can simulate the structural component behaviors in detail and provide the results with high accuracy, however, their modelling procedures are relatively complex, as the same time, they include a large number of nonlinear elements and are not easy to converge during the nonlinear analysis, especially for the collapse analysis, in addition, they also require the large computational efforts. Different from an individual structure, the number of regional buildings is excessive. Therefore, the above disadvantages of the structural refined finite element models cause them be evidently infeasible for the regional seismic collapse analysis. The macro-scale simplified mechanical models (Chen 2008, Han 2010, Shafei 2011, Penna 2014, Hamidia 2014 and Li 2017) include the structural prototype model generated by the structural component hysteretic models, the structural multi-degree-of-freedom shear model constituted by the inter-story hysteretic models of each story, and the structural equivalent single-degree-of freedom (ESDOF) model. The ESDOF model requires the smallest computational effort compared to other two models and is preferred for seismic collapse performance analysis of regional structures.

Some works have been made to establish the structural ESDOF model applicable for the seismic collapse analysis for the individual URM structure and RC frame structure. Prior studies (Park 1985, Haselton 2008a and Haselton 2008b) indicated that, from the view of structural inherent mechanical performance, the deterioration behaviors of structural components due to accumulation damage under seismic excitations are the most primary source of structural collapse (Casolo 2007, Wilding 2017 and Yekrangnia 2017). Furthermore, several researchers (Ibarra 2005, Shi 2014, Lignos 2011a, Lignos 2011b, Adam 2012) analyzed the contribution of different types of deterioration behaviors to structural collapse, and pointed that the monotonic strength deterioration is the primary source of structural collapse under the ground motions with a few obvious large cycles, and the cyclic strength deterioration has an important effect on the structural collapse when encountering the ground motions with a large number of cycles. Therefore, the ESDOF model used for seismic collapse analysis should can correctly simulate the monotonic strength deterioration and cyclic strength deterioration behaviors. Several ESDOF models capable of simulating deterioration behaviors have been developed by utilizing the hysteretic rules from the structural components (Han 2010 and Shafei 2011). The ESDOF model developed by adopting the hysteretic rule from the Ibarra-Krawinkler (IK) model is relatively accurate among the different models because it considers all the important strength and stiffness deterioration behaviors observed in the collapse experiments.

Although the reliable hysteretic rule pattern of the ESDOF model for collapse analysis already been given, the rational parameter determination method of the

ESDOF model aimed to the regional structures is also needed. Existing studies (Han 2010 and Shafei 2011) often determine the structural ESDOF model parameters by performing the static pushover (SPO) analysis. Because the collapse analysis requires the mechanical behaviors of a structure in the large deformation stage, which causes that the monotonic SPO analysis often encounters the non-convergence situations and needed to be performed repeatedly, furthermore, the determination of the hysteretic parameters also requires the repeated cyclic SPO analysis to match the whole hysteretic response of the prototype structure. From the view of these, the current parameter determination methods are not suitable for the seismic collapse performance prediction of regional structures.

Based on the above background, the structural ESDOF model used for collapse analysis for URM structure and RC frame structure is established. The monotonic backbone curve of the ESDOF model includes the strain-softening branch that can simulate the monotonic strength deterioration behaviors, and the hysteretic rule adopts the cyclic deterioration rule from the IK model that can comprehensive considers different types of cyclic deterioration behaviors. These practices assure that the established structural ESDOF model has the correctly simulation of the deterioration behaviors under monotonic and cyclic loading paths. Utilizing the assumption of rigid plane for structural floor slab, the basis theory of SPO analysis, and the empirical statistics of experimental data of URM walls and RC columns, a simplified approach to determine the structural ESDOF model parameters based on the hysteretic model parameters of structural components is proposed, avoiding the repeatedly SPO analysis procedures required in previous studies. The accuracy of the proposed ESDOF model is verified by the pseudo-static collapse experiment of an RC frame structure.

2. BASIS THEORY OF ESDOF MODEL FOR COLLAPSE ANALYSIS

2.1 Monotonic backbone curve

The monotonic backbone curve of the ESDOF model represents the global monotonic response of a multistory structure. Previous studies (Han 2010 and Shafei 2011) often obtain the monotonic backbone curve by performing the static pushover (SPO) analysis of a multistory structure. Experimental studies (Haselton 2007 and Haselton 2008a) exhibited that the occurrence of structural collapse approximately corresponds to the zero base shear force of a structure, i.e. the structure has no more resistance against lateral loads. Thus, the lateral loading displacement adopted to perform the SPO analysis should be continuously increased until the structural global force-displacement curve reaches the point of zero base shear force.

For the first-mode-dominated structure, such as URM structure and RC frame structure mainly distributed in low- and median-story buildings, the lateral loading pattern proportional to the first mode shape times the story masses $\boldsymbol{F} = \boldsymbol{M}\boldsymbol{\phi}_1$ is preferred to perform the SPO analysis, and the conversion relations between the monotonic backbone curve and the global force-displacement curve are $F^* = F_b/\Gamma_1$ and $\delta^* = \delta_t/\Gamma_1$, in which, F_b and δ_t respectively are the base shear force and top displacement of the structure, F^* and δ^* respectively are the force and displacement of the ESDOF model. $\Gamma_1 = \phi_1 \boldsymbol{M}\boldsymbol{I} / \phi_1 \boldsymbol{M}\boldsymbol{I}$ is the first-mode participation factor, where ϕ_1 is the first-mode shape vector, $\boldsymbol{M}$ is the diagonal mass matrix, and $\boldsymbol{I}$ is the unit vector.

The initial monotonic backbone curve obtained by the SPO analysis is smooth. For the ease of numerical implementation of the ESDOF model, the initial monotonic backbone curve is usually changed into a tri-linear model by some idealization procedures (Han 2010), as shown in Fig.1. The idealized tri-linear monotonic backbone consists of an elastic segment, a strain-hardening segment, and a strain-softening segment, in which the softening segment can simulate the strength deterioration in monotonic loading path that is critical for modeling structural collapse. The backbone curve parameters incorporates the elastic stiffness K_e^*, yield strength F_y^*, yield displacement δ_y^*, hardening stiffness K_s^*, peak strength F_c^*, peak displacement δ_p^*, the softening stiffness K_c^*, and ultimate displacement δ_u^*.

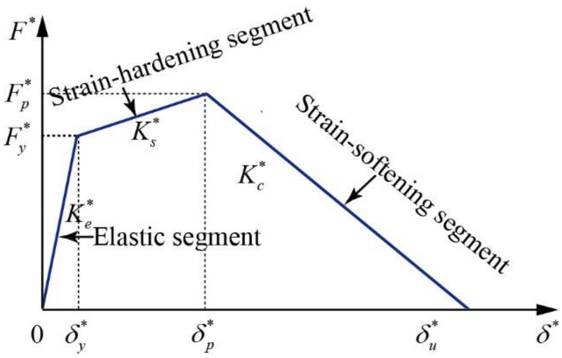

Fig.1 Monotonic backbone curve

2.2 Hysteretic Rule Considering Cyclic Deterioration Behaviors

The hysteretic rule of the ESDOF model reflects the global load-displacement relation of the structures under cyclic loading. Because the strength and stiffness deterioration behaviors of structural components from the accumulation damage under seismic excitations are the most primary source of structural collapse, and the hysteretic rule of the ESDOF model used for collapse analysis should have capacity to simulate all the important deterioration behaviors during structural collapse. Considering the requirement for collapse performance assessment, Ibarra et al (2005) developed the I-K model that integrate all-important cyclic deterioration phenomena by analyzing the monotonic load-displacement response and the superimposed quasi-static cyclic response of the "identical" plywood shear wall panels. In view of this, the hysteretic rule from I-K model is suitable to the ESDOF model for collapse analysis.

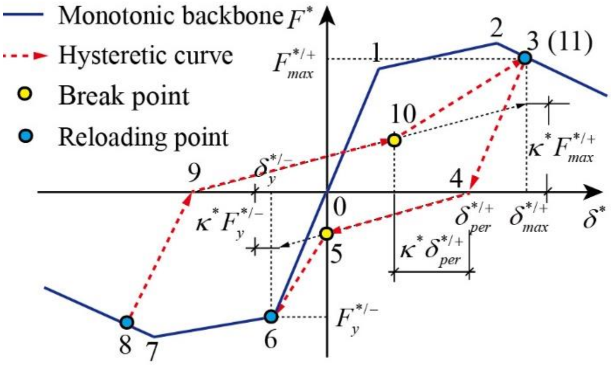

Fig. 2 Pinching hysteretic rule

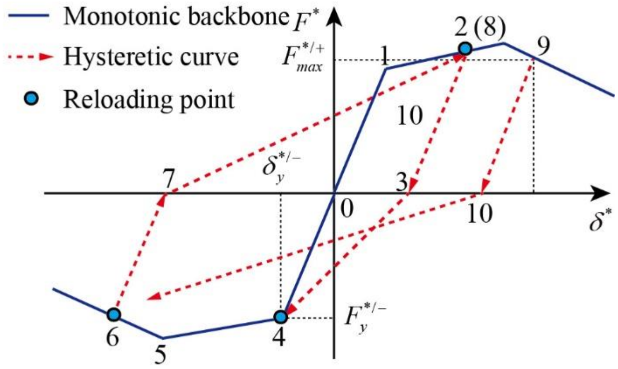

Fig. 3 Peak-oriented hysteretic rule

The hysteretic rule from I-K model is composed of two parts, basis hysteretic rule and cyclic deterioration rule, in which the former rule has three types, bilinear, peak-oriented and pinched model, for applying to different types of building structures. In the URM structure, its URM walls often fail in shear mode and exhibit significant pinching behavior, consequently, the pinched hysteretic model is preferred, as shown in Fig.2; in the RC frame structure, pinching behavior is not a dominant factor for RC columns with flexural failure, and the peak-oriented hysteretic model is feasible, as shown in Fig.3. The reloading path in these two basic hysteretic rule always targets the previous maximum displacement, and thus the deterioration of reloading stiffness could be simulated. For this pinched hysteretic model, the reloading path consists into two parts due to the existence of break points, this practice could achieve the simulation of pinching behaviours. The break point is a function of the maximum permanent deformation δ^*_{per} and the maximum strength F^*_{max} experienced in the loading direction and is controlled by the parameter κ^*. The smaller value of parameter κ^* means more evident pinching behavior, and when $\kappa^* = 1.0$, the pinching behavior is not existed, such as peak-oriented hysteretic rule.

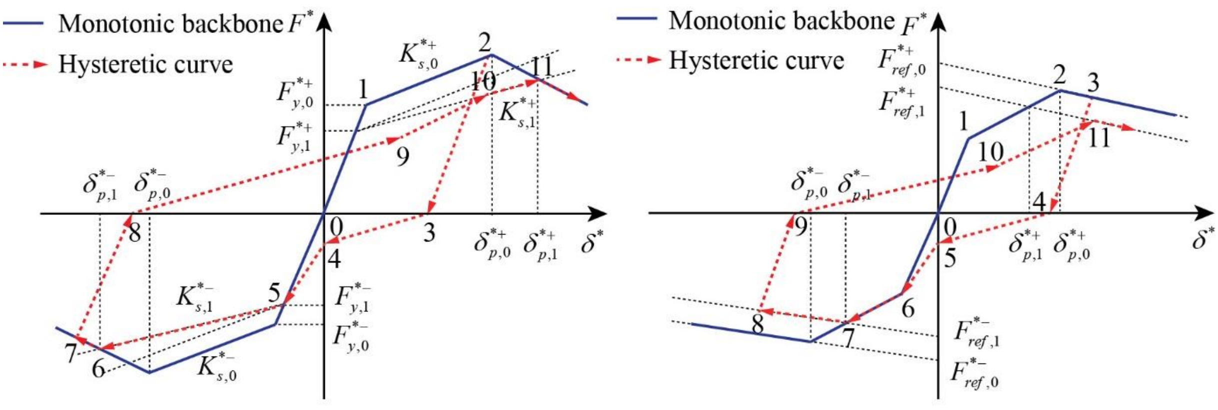

(a) Basic strength deterioration

(b) Post-capping strength deterioration

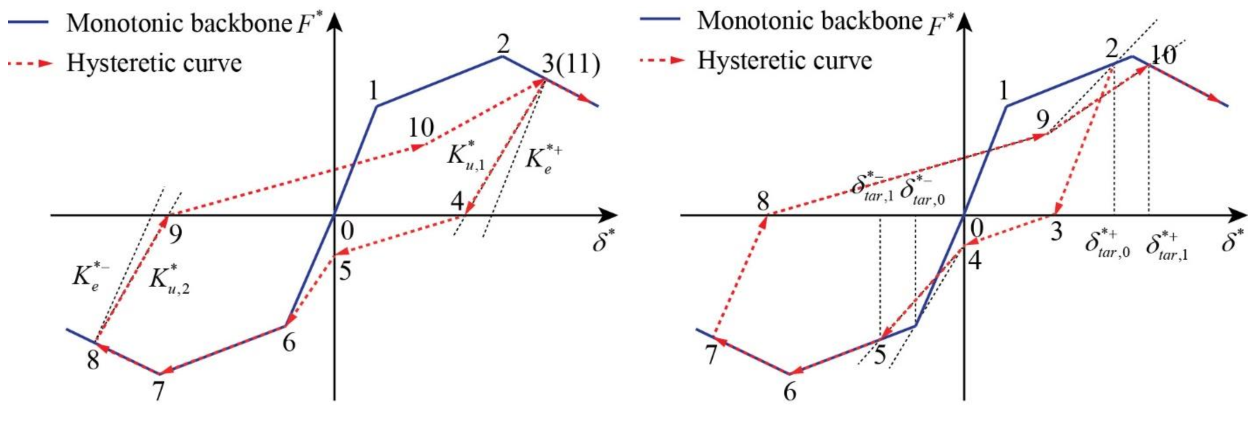

(c) Unloading stiffness deterioration (d) Accelerated reloading stiffness deterioration

Fig. 4 Cyclic deterioration modes

The cyclic deterioration rules include four cyclic deterioration modes, as shown in Fig.4: the basic strength deterioration (deterioration from yield strength and strain-hardening stiffness), post-capping strength (the intersection of the vertical axis with the projection of the softening stiffness branch) deterioration, unloading stiffness deterioration, and accelerated reloading stiffness deterioration. The deterioration rate of these four cyclic deterioration modes are often deemed same and is controlled by the energy-based rule developed by Rahnama and Krawinkler (1993). According to this rule, it is assumed that every structural ESDOF model possesses a reference inherent hysteretic energy dissipation, regardless of the loading history, and the cyclic deterioration in ith loading cycle is defined by parameter β_i^*:

$$\beta_i^* = \frac{E_i^*}{E_t^* - \sum_{j=1}^{i} E_i^*} \tag{1}$$

in which, E_i^* is the hysteretic energy dissipated in ith cycle; $\sum_{j=1}^{i} E_i^*$ is the cumulative hysteretic energy dissipated in all past cycles; E_t^* is the reference inherent hysteretic energy dissipation, which is the function of the elastic strain energy at yielding, expressed as follows:

$$E_t^* = \gamma^* F_y^* \delta_y^* \tag{2}$$

where parameter γ^* is the reference hysteretic energy dissipation capacity. The smaller value of parameter γ^* causes the faster cyclic deterioration rate, and when γ^* approaches infinite, the cyclic deterioration will be not existed. With Eq. (1) and Eq. (2), the deteriorated yield strength $F_{y,i}^*$, hardening stiffness $K_{s,i}^*$, post-capping strength $F_{cap,i}^*$, unloading stiffness $K_{u,i}^*$, and accelerated reloading stiffness that is simulated by increasing the reloading target displacement $\delta_{tar,i}^*$, are calculated by the following equations:

$$F_{y,i}^{*}=(1-\beta_i^{*})F_{y,i-1}^{*} \qquad K_{s,i}^{*}=(1-\beta_i^{*})K_{s,i-1}^{*} \tag{3}$$

$$F_{ref,i}^{*}=(1-\beta_i^{*})F_{ref,i-1}^{*} \qquad K_{u,i}^{*}=(1-\beta_i^{*})K_{u,i-1}^{*} \qquad \delta_{tar,i}^{*}=(1-\beta_i^{*})\delta_{tar,i-1}^{*} \tag{4}$$

2.3 Common Procedure of Determinating ESDOF Model Parameters

According the above description of ESDOF model, it is known that three types of parameters needed to be determined for achieving the structural seismic collapse analysis using the ESDOF model.

(1) Structural basic characteristic parameters, including diagonal mass matrix $\boldsymbol{M}$ and elastic stiffness matrix $\boldsymbol{K}_e$. With those parameters, the fundamental period T, first-mode shape vector $\boldsymbol{\phi}_1$, the first-mode lateral loading pattern $\boldsymbol{F}=\boldsymbol{M}\boldsymbol{\phi}_1$, and first-mode participation factor $\Gamma_1=\phi_1\boldsymbol{MI}/\phi_1\boldsymbol{MI}$ can be calculated.

(2) Monotonic backbone parameters of ESDOF model, including yield strength F_y^*, yield displacement δ_y^*, peak strength F_c^*, peak displacement δ_p^*, and ultimate displacement δ_u^*. Using these parameters, other backbone parameters, the elastic stiffness K_e^*, hardening stiffness K_s^*, and the softening stiffness K_c^* can be determined.

(3) Hysteretic rule parameters of ESDOF model, including pinching parameter κ^* and hysteretic energy dissipation parameter γ^*.

For a specific structure, its structural characteristic parameters are often easily obtained. However, the determination of monotonic backbone parameters and hysteretic rule parameters is relatively complex. The detailed steps of determining the ESDOF model parameters are shown in Fig.5. The determination of monotonic backbone parameters requires both monotonic SPO analysis and idealization procedures. Because the backbone curve for collapse analysis need include the whole strain-softening segment from the peak strength to zero lateral resistance, which leads that the monotonic SPO analysis often encounter non-convergence situations and is repeatedly performed with many times. After the determination of backbone parameters is completed, the hysteretic rule parameters are determined by continuously adjusting parameters κ^* and γ^* to fit the structural hysteretic curves. Similarly to backbone parameters, this procedure also need repeated cyclic SPO analysis with several times.

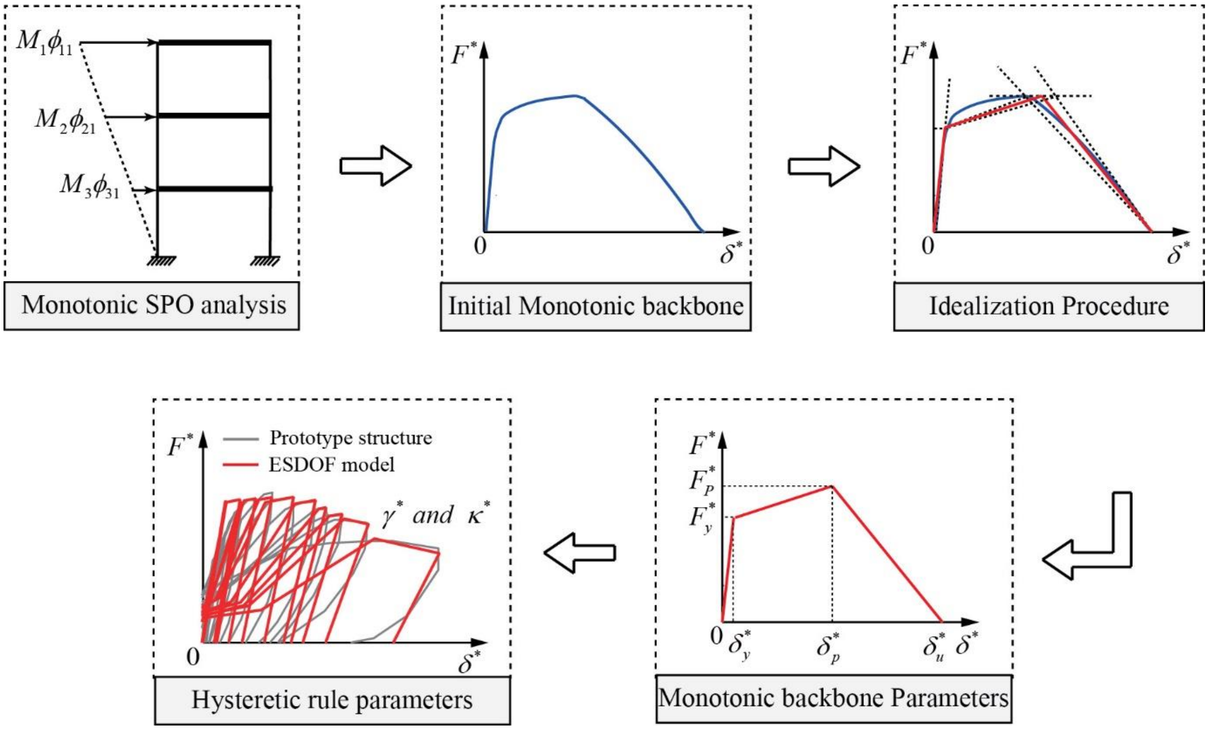

Fig. 5 Common procedure of determining the ESDOF model parameters

3. DETERMINATION OF MONOTONIC BACKBONE PARAMETERS

Different from the seismic collapse analysis of an individual building, the number of buildings in a region can be excessive, which makes previous determination procedure of the ESDOF model parameters is inapplicable due to its complexity. Therefore, this study develops a relatively simple method to determine the structural ESDOF model parameters based on the structural component hysteretic model parameters, avoiding the SPO analysis and the backbone curve idealization procedures, the detailed introduction is as follow.

Existing literatures (Xiong 2017 and Lu 2017) proved that the multiple degrees of freedom shear model can well capture the seismic nonlinear responses of low- and multi-story buildings which are dominated by the inter-story shear deformation. Some assumptions are adopted in this model: the floor slab on each story is deemed as a rigid plane; the mass of each story is concentrated on its floor slab and is represented by a mass point; the rotational deformation of the floor slab on each story is neglected. Previous studies have shown that the tri-linear backbone curve can also accurately represent the structural inter-story behavior as well as the component behavior. Thus, on the basis of the assumptions from the multiple degrees of freedom shear model, the inter-story tri-linear monotonic backbone parameters can be easily obtained based on the monotonic backbone parameters from the hysteretic models of components in each story. For the RC frame and URM structures, the calculation methods of monotonic backbone parameters for RC columns and URM walls have been given by Ibarra et al (2008b) and Yu et al (2022). Specific determination process of the inter-story tri-linear monotonic backbone parameters is described as follows.

According to the rigid plane assumption of the floor slab, all the components of each story have the same lateral displacement that also equals to the inter-story lateral displacement; the inter-story lateral strength is equal to the sum of the lateral strength of all components in the same lateral displacement. The lateral mechanical characteristics of components in each story are represented by the hysteretic models. When the inter-story displacement exceeds the smallest yield displacement of all inter-story components, the inter-story force-displacement curve starts to occur inflection and this story enters the nonlinear stage. Thus, the inter-story yield strength $F_{y,j}^{story}$ and yield displacement $\delta_{y,j}^{story}$ of the jth story are estimated based on this first inflection point. Mathematically, $\delta_{y,j}^{story} = \min(\delta_{y,i,j})$, and $F_{y,j}^{story} = \delta_{y,j}^{story} \sum K_{e,i,j}$, where $\delta_{y,i,j}$ and $K_{e,i,j}$ are the yield displacement and elastic stiffness of the ith component in the jth story, respectively. The inter-story monotonic peak strength $F_{p,j}^{story}$ and peak displacement $\delta_{p,j}^{story}$ in the jth story are estimated by the point of maximum inter-story monotonic lateral strength. The inter-story monotonic ultimate strength $F_{u,j}^{story}$ in the jth story is $F_{u,j}^{story} = 0$. The inter-story monotonic ultimate displacement $\delta_{u,j}^{story}$ in the jth story is estimated by the equivalent area rule of the monotonic backbone. Specifically, $A_{mono,j}^{story} = \sum A_{mono,i,j}$, where $A_{mono,j}^{story}$ and $A_{mono,i,j}$ respectively are the monotonic backbone curve area of the jth story and the monotonic backbone curve area of the ith component in the jth story. Experiencing above procedure, the inter-story monotonic backbone parameters can be determined, the schematic diagram comparing with the initial inter-story monotonic backbone curve generated by the component hysteretic models is shown in Fig. 6.

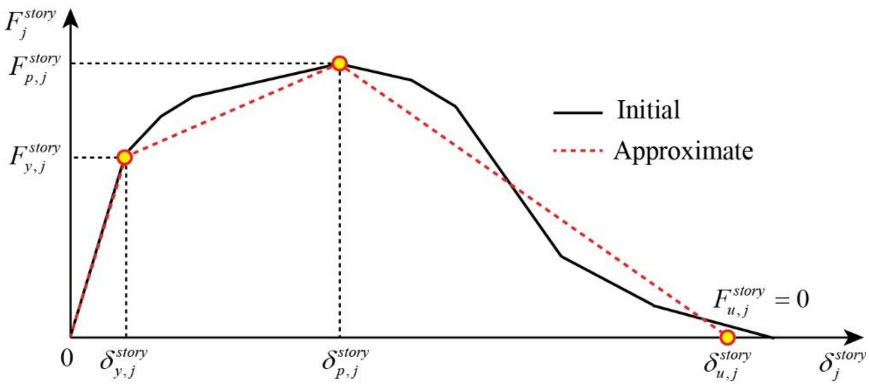

Fig. 6 Initial and approximate inter-story monotonic backbone curves

Based on above-determined inter-story monotonic backbone parameters, by further using the principle of the SPO analysis, the monotonic backbone parameters of the ESDOF model are determined. Detailed procedure is as follows.

$\boldsymbol{F_y^*}$ **and** $\boldsymbol{\delta_y^*}$**.** In the SPO analysis, the lateral loading pattern for the first-mode dominated structure $\{M_1\phi_{11}, M_2\phi_{21}, \cdots, M_j\phi_{j1}, \cdots, M_n\phi_{n1}\}^T$ is always proportional to the first mode shape times the story masses. Therefore, according to the already known inter-story yield strength of each story, and the jth story that firstly reaches its inter-story yield point in the SPO analysis can be inferred. Mathematically:

$$\max\left\{\frac{\sum_{i=1}^{n} M_i\phi_{i1}}{F_{y,1}^{story}}, \frac{\sum_{i=2}^{n} M_i\phi_{i1}}{F_{y,2}^{story}}, \cdots, \frac{\sum_{i=j}^{n} M_i\phi_{i1}}{F_{y,j}^{story}} \cdots, \frac{\sum_{i=n}^{n} M_i\phi_{i1}}{F_{y,n}^{story}}\right\} \tag{5}$$

where $F_{y,j}^{story}$ is the inter-story yield strength of the jth story, and $j=1,2,\cdots,n$. After that, using the inter-story yield strength $F_{y,j}^{story}$, the yield strength F_y^* and yield displacement δ_y^* of the ESDOF model are determined in accordance with the following equations. Fig.7 shows the possible inter-story force-displacement relation of other stories when the jth story reaches its inter-story yield strength point.

$$F_y^* = \frac{1}{\Gamma_1}\cdot\frac{F_{y,j}^{story}}{\sum_{i=j}^{n} M_i\phi_{i1}}\sum_{i=1}^{n} M_i\phi_{i1} \tag{6}$$

$$\delta_{y,j,k}^{story} = \begin{cases} F_{y,j,k}^{story}/K_{e,k}^{story} & F_{y,j,k}^{story} < F_{y,k}^{story}\ (elastic\ state) \\ \delta_{y,k}^{story} & F_{y,j,k}^{story} = F_{y,k}^{story}\ (yield\ point) \end{cases} \tag{7}$$

$$\delta_y^* = \left(\delta_{y,j,1}^{story} + \delta_{y,j,2}^{story} + \cdots + \delta_{y,j,k}^{story} + \cdots + \delta_{y,j}^{story} + \cdots + \delta_{y,j,n}^{story}\right)/\Gamma_1 \tag{8}$$

Parameters $\delta_{y,j,k}^{story}$ and $F_{y,j,k}^{story} = \left(F_{y,j}^{story}/\sum_{i=j}^{n} M_i\phi_{i1}\right)\sum_{i=k}^{n} M_i\phi_{i1}$ respectively are the inter-story displacement and inter-story strength of the kth story when the jth story reaches its inter-story yield strength point, and $k=1,2,\cdots,j-1,j+1,\cdots,n$. Parameter $\delta_{y,j}^{story}$ is the inter-story yield displacement of the jth story.

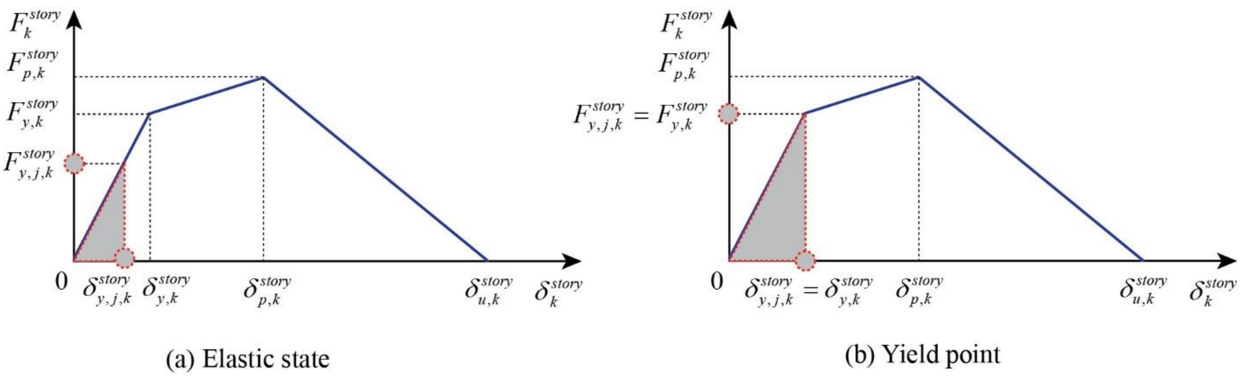

Fig.7 The possible inter-story force-displacement relation of other stories when the jth story reaches its inter-story yield strength point.

F_p^* and δ_p^*. Similarly to the yield parameters, the jth story that firstly reaches its inter-story monotonic peak strength point in the SPO analysis can be inferred by again utilizing the principle of the constant lateral loading pattern and the already known inter-story monotonic peak strength of each story. Then using the inter-story monotonic peak strength $F_{p,j}^{story}$ in jth story, the monotonic peak strength F_p^* of the ESDOF model is determined. Mathematically, Eq. (5) and Eq. (6) are also applied except for replacing the $F_{y,j}^{story}$ with $F_{p,j}^{story}$. In the SPO analysis, the performance states of other stories in addition to the jth story can be elastic state or strain-hardening state when the jth story reaches its inter-story monotonic peak strength point. Therefore, the performance state of each story is need to be inferred firstly to obtain the inter-story displacement of each story, and then the inter-story displacement of each story is summed to determine the monotonic peak displacement δ_p^* of the ESDOF model. Fig.8 shows the possible inter-story force-displacement relation of other stories when the jth story reaches its inter-story monotonic peak strength point. Specific mathematical expressions are as follows.

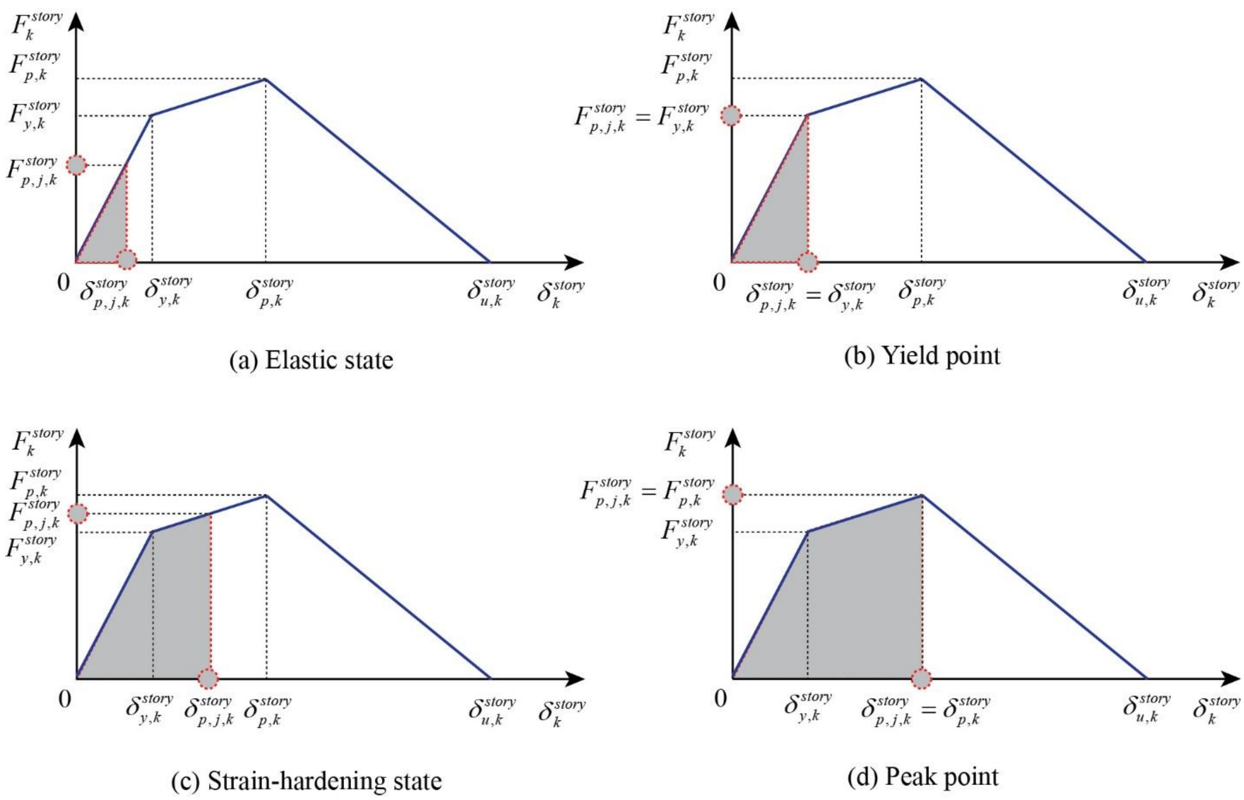

Fig.8 The possible inter-story force-displacement relation of other stories when the jth story reaches its inter-story monotonic peak strength point.

$$\delta_{p,j,k}^{story} = \begin{cases} F_{p,j,k}^{story} / K_{e,k}^{story} & F_{p,j,k}^{story} < F_{y,k}^{story} \quad (elastic \ \ state) \\ \delta_{y,k}^{story} & F_{p,j,k}^{story} = F_{y,k}^{story} \quad (yield \ \ point) \\ \delta_{y,k}^{story} + \left(F_{p,j,k}^{story} - F_{y,k}^{story} \right) / K_{s,k}^{story} & F_{y,k}^{story} < F_{p,j,k}^{story} < F_{p,k}^{story} \quad (strain-hardening \ \ state) \\ \delta_{p,k}^{story} & F_{p,j,k}^{story} = F_{y,k}^{story} \quad (yield \ \ point) \end{cases} \tag{9}$$

$$\delta_p^* = \left(\delta_{p,j,1}^{story} + \delta_{p,j,2}^{story} + \cdots + \delta_{p,j,k}^{story} + \cdots + \delta_{p,j}^{story} + \cdots + \delta_{p,j,n}^{story}\right) \Big/ \Gamma_1 \tag{10}$$

Parameters $\delta_{p,j,k}^{story}$ and $F_{p,j,k}^{story} = \left(F_{p,j}^{story} \Big/ \sum_{i=j}^{n} M_i \phi_{i1}\right) \sum_{i=k}^{n} M_i \phi_{i1}$ respectively are the inter-story displacement and inter-story strength of the kth story when the jth story reaches its inter-story peak strength point, and $k = 1, 2, \cdots, j-1, j+1, \cdots, n$; parameter $\delta_{p,j}^{story}$ is the inter-story peak displacement of the jth story.

F_u^* and δ_u^*. The monotonic ultimate strength of the ESDOF model is designed as $F_u^* = 0$. In the SPO analysis, for the jth story that firstly reaches its inter-story monotonic peak strength point, with the continually increased lateral loading displacement, this story will also firstly enter the strain-softening stage, and the inter-story strength starts to degenerate with the increased lateral displacement, finally, this story loses its lateral resistance completely, and structural collapse occurs. Because of the constant lateral loading pattern adopted in the SPO analysis, the inter-story strength of other stories except for the jth story also synchronously decrease to the point of zero strength. At this moment, the performance states of these stories related to such point of zero strength can be elastic state or strain-hardening state or strain-softening state. Fig.9 shows the possible inter-story force-displacement relation of other stories when the jth story reaches its inter-story monotonic ultimate displacement point.

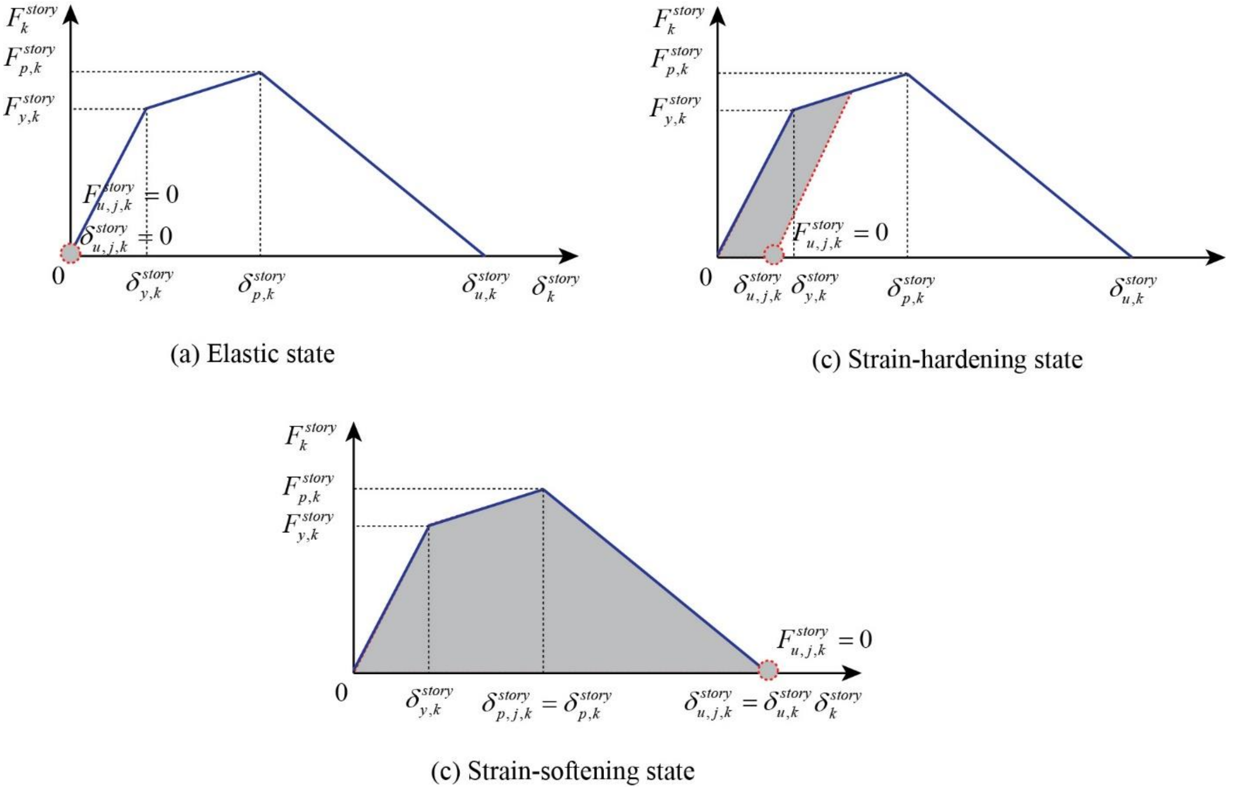

(a) Elastic state

(c) Strain-hardening state

(c) Strain-softening state

Fig.9 The possible inter-story force-displacement relation of other stories when the jth story reaches its inter-story monotonic ultimate displacement point.

For an example of the kth story, $k = 1, 2, \cdots, j-1, j+1, \cdots, n$, when the kth story is in the elastic stage or strain-hardening state, the zero inter-story strength of this story is due to its unloading behavior, and when the kth story is in the strain-softening state, it means that this story reaches its inter-story monotonic peak strength point at the same time with the jth story and also occur strength degenerate in the strain-softening stage, leading to the zero inter-story strength. Therefore, the performance state of each story is inferred firstly so as to obtain the inter-story displacement of each story. Later, the inter-story displacement of each story is summed to obtain the monotonic ultimate displacement δ_u^* of the ESDOF model. Mathematical expressions are as follows:

$$\delta_{u,j,k}^{story} = \begin{cases} 0 & F_{p,j,k}^{story} \le F_{y,k}^{story} \quad (elastic \;\; state) \\ \delta_{p,j,k}^{story} - F_{p,j,k}^{story} / K_{e,k}^{story} & F_{y,k}^{story} < F_{p,j,k}^{story} < F_{p,k}^{story} \quad (strain-hardening \;\; state) \\ \delta_{u,k}^{story} & F_{p,j,k}^{story} = F_{p,k}^{story} \quad (stran-softening \;\; state) \end{cases} \tag{11}$$

$$\delta_u^* = \left(\delta_{u,j,1}^{story} + \delta_{u,j,2}^{story} + \cdots + \delta_{u,j,k}^{story} + \cdots + \delta_{u,j}^{story} + \cdots + \delta_{u,j,n}^{story} \right) / \Gamma_1 \tag{12}$$

where, $\delta_{u,j,k}^{story}$ is the inter-story displacement of kth story when the jth story reaches its monotonic ultimate displacement point of zero lateral resistance; $\delta_{u,j}^{story}$ is the inter-story monotonic ultimate displacement of jth story. Experiencing above procedure, the monotonic backbone parameters of the structural ESDOF model can be determined, and the schematic diagram comparing with the original monotonic backbone curve obtained by the SPO analysis for the numerical model of prototype structure generated by the component hysteretic models is shown in Fig. 10.

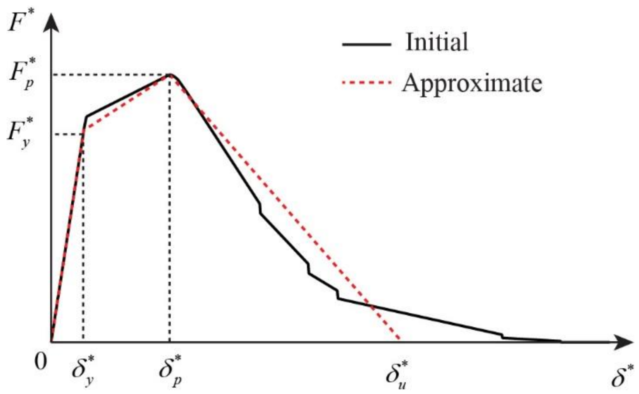

Fig. 10 Original and approximate monotonic backbone curves of the structural ESDOF model

4. DETERMINATION OF HYSTERETIC RRLE PARAMETERS

Hysteretic rule parameters of the ESDOF model include the hysteretic energy dissipation parameter γ^* controlling the cyclic deterioration rate and the pinching parameter κ^* simulating the pinching behavior. It is known that a high positive correlation is existed between the ductility capacity and hysteretic energy dissipation capacity of a structure. The monotonic ductility capacity μ^* of a structure can be easily obtained by the monotonic backbone parameters of the structural ESDOF model. Consequently, the parameter γ^* of the ESDOF model also can be conveniently determined with the $\mu^*-\gamma^*$ empirical relationship. Previous studies (Fajfar 1992 and Zhai 2013) exhibit that, the empirical model of ductility and hysteretic energy dissipation in the component level is also applicative for the whole structure. Therefore, for RC frame and URM structures, this study adopts their empirical relationships from the experimental data of RC columns and URM walls to determine γ^* value of the ESDOF model. Detailed descriptions about the $\mu-\gamma$ empirical relationships for RC columns and URM walls have been given by Li et al (2019), and this paper only shows the $\mu^*-\gamma^*$ empirical models as the following expressions, in which, the monotonic ductility capacity is defined as $\mu^*=\delta_p^*/\delta_y^*$.

$$\gamma^* = \begin{cases} 0.60(\mu^*)^2 + 4.95\mu^* + 30.97 & RC\ frame \\ 0.72(\mu^*)^2 + 4.88\mu^* + 4.50 & URM\ structure \end{cases} \tag{13}$$

Considering that the pinching behaviour of structural components has a very small effect on the seismic collapse performance (Ibarra 2005). Yu et al (2022) determines the pinching parameter of the URM wall by a constant value of 0.70. From this, this paper assumes that the whole URM structure also has the same degree of pinching behavior with its components, and the pinching parameter $\kappa^*=0.70$ is used for the ESDOF model of the URM structure.

5. VERIFICATION BY THE PSEUDO-STATIC COLLAPSE EXPERIMENTS OF RC FRAME

To validate the accuracy of the developed ESDOF model to predict the global mechanical behaviors during structural collapse, comparisons with the experimental data of the collapse test of the RC frame are conducted.

The collapse test used in this study comes from the pseudo-static collapse test conducted by Xie et al. (2015), which is a plan RC frame with 3-span spaced at 3.0 m, 3-story with a height of 1.65 m. Test setups of the frame are illustrated in Fig. 11. Constant vertical concentrated loads are applied to the top of the frame, in which the proportion of vertical loads for the side column and middle column is 1:2. The cyclic lateral loads with a proportion of 18:2:1 are applied at the third, second, and first story of the frame, respectively. The lateral loading process is controlled by the top displacement.

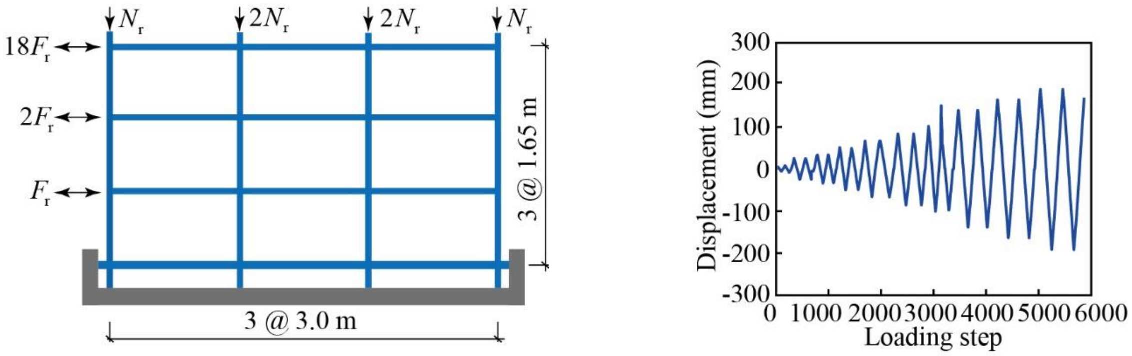

(a) Load pattern (b) lateral loading protocol.

Fig.11 Test setup of the overall frame.

The ESDOF model parameters of the RC frame test are described as follow. The mass of each story is derived by the vertical concentrated loads applied at the test frame, and generating the structural diagonal mass matrix $\boldsymbol{M}$. Based on the assumption of rigid plane of each story, the inter-story elastic stiffness of each story is solved by summing the elastic stiffness of all RC columns of each story and producing the structural elastic stiffness matrix $\boldsymbol{K}_e$. Subsequently, the fundamental period T, first-mode shape vector ϕ_1, the first-mode lateral loading pattern $\boldsymbol{F} = \boldsymbol{M}\phi_1$, and first-mode participation factor $\Gamma_1 = \phi_1 \boldsymbol{MI} / \phi_1 \boldsymbol{MI}$ of the RC frame test are calculated. Adopting the calculation equations from Ibarra et al (2005), the monotonic backbone parameters of the RC columns for the frame test are solved, as shown in Tab. 1. According the determination procedure of ESDOF model parameters proposed in this paper, the ESDOF model parameters of the RC frame test are quickly obtained, and the results are shown in Tab. 2.

Tab. 1 Parameter values of the I-K models of the columns for the test RC frame

Story	Column	F_y (KN)	δ_y (mm)	F_p (KN)	δ_p (mm)	δ_u (mm)
1-3	Side	39	5.3	46	55.3	151.9
	Middle	57	5.9	66	51.2	143.5

Tab. 2 Parameter values of the I-K models of the beams for the test RC frame

F_y^* (KN)	δ_y^* (mm)	F_p^* (KN)	δ_p^* (mm)	δ_u^* (mm)	μ^*	γ^*
170	45	190	315	500	7.0	91.3

The IK model has been implemented in the Open System for Earthquake Engineering Simulation (OpenSees) analysis software, and thus the modelling of the ESDOF model for the RC frame test with parameters in Tab. 2 is completed by the lumped plasticity element in OpenSees. Applied to the same lateral loading protocol in Fig. 11(b), the nonlinear analysis of the ESDOF model is performed. Comparisons between the global mechanical behaviors of the RC frame obtained from the experiment and predicted by the ESDOF model are presented in Fig. 12. The results indicate that, the predicted force-displacement curve and its associated envelope curve by the ESDOF model have a close agreement with the experimental data, the occurred deterioration bahaviors in the large deformation stage (the roof displacement of the RC frame surpasses 139 mm) of tested RC frame during its collapse are simulated with a good accuracy.

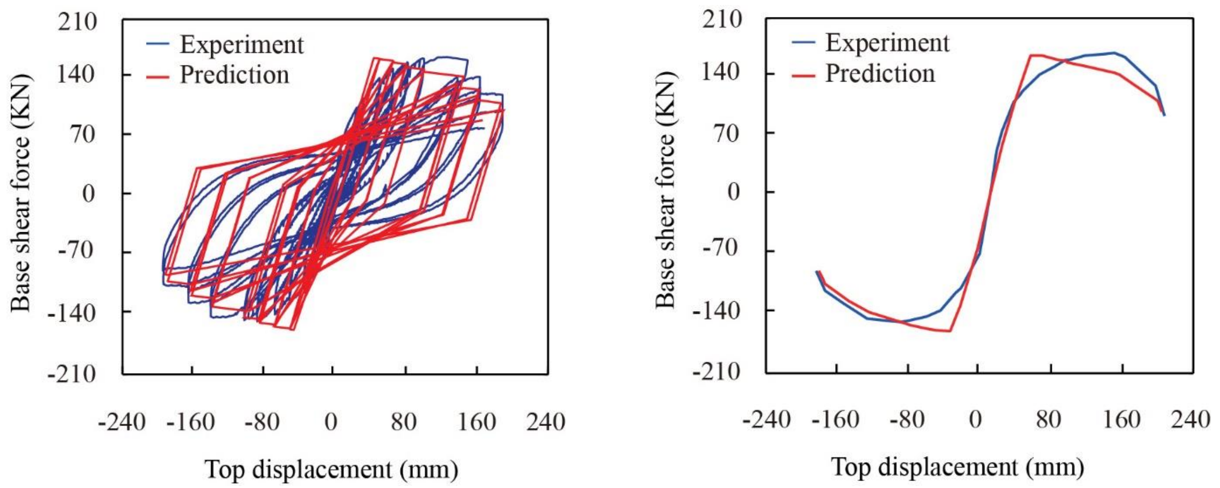

Fig.12 Comparison of the tested and predicted global force-displacement curve of the RC frame

During the experiment of the overall RC frame, some key damage state that represent the different damage degrees of the test RC frame are defined based on test observations, as signed in Fig. 13. Comparison of the base shear force at different damage state obtained by the experiment and the numerical modelling of the ESDOF model are shown in Tab. 3. The ratios of the experimental to predicted base shear force from the moderate damage state to the near-collapse state are in the range of 0.90-1.09, very closed to 1.0, indicating that the proposed ESDOF model can provide a good prediction of the global mechanical behavior during the collapse of RC frame.

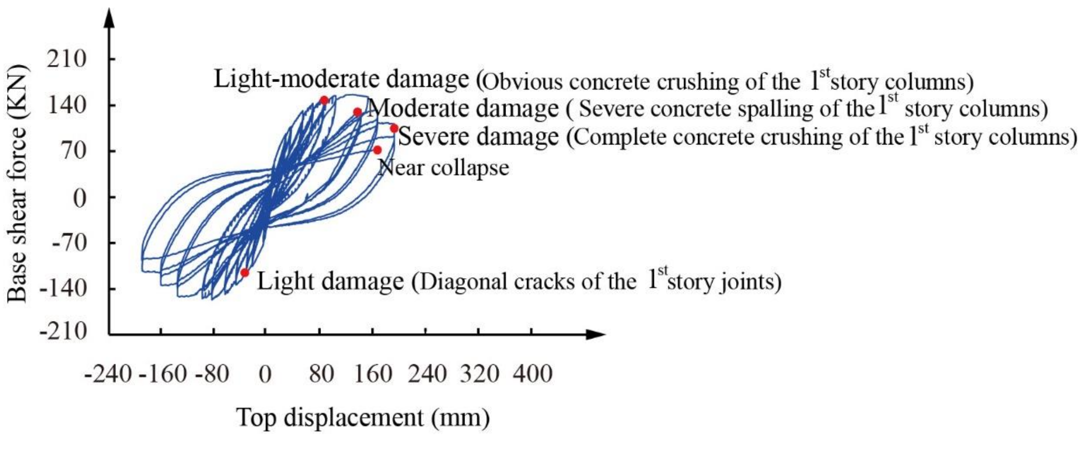

Fig.13 Damage state points of during the collapse of tested RC frame.

Tab. 3 Ratio of the experimental to predicted base shear force at different damage state

Light	Light-moderate	Moderate	Severe	Near -collapse
0.821	1.00	1.03	1.09	0.90

6. CONCLUSIONS

The parameter determination method of the structural ESDOF model applicable for the regional seismic collapse performance prediction of the low- and multi-story URM and RC frame structures is proposed in this study. The structural ESDOF model parameters are quickly solved based on the hysteretic model parameters of structural components, which is very simple and convenient compared to the previous studies required the repeated SPO analysis procedures.

The accuracy of performing collapse performance prediction using the proposed structural ESDOF model is verified by the pseudo-static collapse experiment of an RC frame structure. The predicted global force-displacement response of the RC frame has a well agreement with the experimental results, demonstrating the feasible of this proposed ESDOF model to perform the structural global seismic collapse performance prediction.

REFERENCES

Adam, C. and Jäger, C. (2012), “Simplified collapse capacity assessment of earthquake excited regular frame structures vulnerable to P-delta.” *Eng. Struct*., Vol. **44**(8), 159-173.

Bothara, J.K., Dhakal, R.P. and Mander, J.B. (2010), “Seismic performance of an unreinforced masonry building: an experimental investigation.” *Earthq. Eng. Struct. Dyn*., Vol. **39**(1), 45-68.

Chaimoon, K. and Attard, M.M. (2007), “Modeling of unreinforced masonry walls under shear and compression.” *Eng. Struct*., Vol. **29**(9), 2056-2068.

Chen, S.Y., Moon, F.L. and Yi, T. (2008), “A macro-element for the nonlinear analysis of in-plane unreinforced masonry piers.” *Eng. Struct*., Vol. **30**(8), 2242-2252.

Casolo, S. and Pena, F. (2007), “Rigid element model for in-plane dynamics of masonry walls considering hysteretic behavior and damage.” *Earthq. Eng. Struct. Dyn*., Vol. **36**(8), 1029-1048.

Dolatshahi, K.M., Aref, A.J. and Yekrangnia M. (2014), “Bidirectional behavior of unreinforced masonry walls.” *Earthq. Eng. Struct. Dyn*., Vol. **43**(15), 2377-2397.

Fajfar, P. (1992), “Equivalent ductility factors, taking into account low-cycle fatigue.” *Earthq. Eng. Struct. Dyn*., Vol. **21**(10), 837-848.

Hamidia, M., Filiatrault, A. and Aref, A. (2014), “Simplified seismic sides way collapse analysis of frame buildings.” *Earthq. Eng. Struct. Dyn*., Vol. **43**(3), 429-448.

Han, S.W., Moon, K.H. and Chopra, A.K. (2010), “Application of MPA to estimate probability of collapse of structures.” *Earthq. Eng. Struct. Dyn*., Vol. **39**(11), 1259-1278.

Haselton, C.B., Liel, A.B. Dean, B.S. Chou, J.H. and Deierlein, G.G. (2007), “Seismic collapse safety and behavior of modern reinforced concrete moment frame buildings.” *ASCE.,* Vol. **249**, 1-14.

Haselton, C.B., Goulet, C.A., Mitrani-Reiser, J., Beck, J.L., Deierlein, G.G., Porter, K.A., Stewarb, J.P. and Taciroglu, E. (2008a), “An assessment to benchmark the seismic performance of a code-conforming reinforced-concrete moment-frame building.” *Report 2007/03*, Pacific Earthquake Engineering Research Center.

Haselton, C.B., Liel, A.B. Lange, S.T. and Deierlein, G.G. (2008b), “Beam-column element model calibrated for predicting flexural response leading to global collapse of RC frame buildings.” *Report 2007/03*, Pacific Earthquake Engineering Research Center.

Ibarra, L.F. and Krawinkler, H.A. (2005), “Global collapse of frame structures under seismic excitations.” *Report 2005/06*, Pacific Earthquake Engineering Research Center.

Ibarra, L.F., Medina, R.A. and Krawinkler, H. (2005), “Hysteretic models that incorporate strength and stiffness deterioration.” *Earthq. Eng. Struct. Dyn*., Vol. **34**(12), 1489-1511.

Lu, X.Z., Ye, L.P., Ma, Y.H. and Tang, D.Y. (2012), “Lessons from the collapse of typical RC frames in Xuankou school during the great Wenchuan earthquake.” *Adv. Struct. Eng*., Vol. **15**(1), 139-153.

Li, G., Dong, Z.Q., Li, H.N. and Yang, Y.B. (2017), “Seismic collapse analysis of concentrically-braced frames by the IDA method.” *Adv. Steel. Constr*., Vol. **13**(3), 273-293.

Lignos, D.G., Chung, Y. Nagae, T. and Nakashima, M. (2011a), “Numerical and experimental evaluation of seismic capacity of high-rise steel buildings subjected to long duration earthquakes.” *Comput. Struct*., Vol. **89**(11), 959-967.

Lignos, D.G., Krawinkler, H. and Whittaker, A. (2011b), “Prediction and validation of sidesway collapse of two scale models of a 4-story steel moment frame.” *Earthq. Eng. Struct. Dyn*., Vol. **40**(7), 807-825.

Lu, X., Tian, Y., Guan, H., and Xiong, C. (2017), “Parametric sensitivity study on regional seismic damage prediction of reinforced masonry buildings based on time-history analysis.” *B. Earthq. Eng*., Vol. **15**, 4791-4820.

Li, G., Yu, L.L and Dong, Z.Q. (2019), “Simplified Collapse Analysis Model for RC Frames with Cyclic Deterioration Behaviors.” *J. Earth. Eng*., Vol. **26**.

Otani, S. (1999), “RC building damage statistics and SDF response with design seismic forces.” *Earthq. Spectra.,* Vol. **15**(3), 485-501.

Penna, A., Lagomarsino, S. and Galasco, A.A. (2014), “Nonlinear macro-element model for the seismic analysis of masonry buildings.” *Earthq. Eng. Struct. Dyn*., Vol. **43**(2), 159-179.

Park, Y.J., and Ang, H.S. (1985), “Mechanistic seismic damage model for reinforced concrete.” *J. Earth. Eng*., Vol. **111**(4), 722-739.

Quiroz, L.G., Maruyama, Y. and Zavala, C. (2014), “Cyclic behavior of Peruvian confined masonry walls and calibration of numerical model using genetic algorithms.” *Eng. Struct*., Vol. **75**(15), 561-576.

Rahnama, M. and H. Krawinkler. (1993), “Effects of soft soil and hysteresis model on seismic demands.” *Report no 108*, Stanford University.

Swinbanks, D. (1995), “Kobe Earthquake shatters faith in engineers.” *Nature*., Vol. **373**(6512), 273-273.

Sandoval, C., Serpell, R., Araya-Letelier, G., and Calderon, S. (2021), “Shear behavior of single- and triple-thickness masonry panels strengthened by bed-joint structural repointing.” *Constr. Build. Mater*., Vol. **286**.

Shakarami, B., Kabir, M.Z. and Sistaninejad, R. (2018), “Parametric study on confined masonry walls subjected to in-plane cyclic loading through numerical modeling.” *AUT J Civil Eng*., Vol. **2**(1), 49-58.

Shafei, B.F., Zareian, and Lignos, D.G. (2011), “A simplified method for collapse capacity assessment of moment-resisting frame and shear wall structural systems.” *Eng. Struct*., Vol. **33**(4), 1107-1116.

Shi, W., Lu, X.Z., Guan, H. and Ye, L.P. (2014), “Development of seismic collapse capacity spectra and parametric study.” *Adv. Struct. Eng*., Vol. **17**(9), 1241-1255.

Wu, C.L., Kuo, W.W., Yang, Y.S., Hwang, S.J., Elwood, K.J., Loh, C.H. and Moehle, J.P. (2009), “Collapse of a non-ductile concrete frame: Shaking table tests.” *Earthq. Eng. Struct. Dyn*., Vol. **38**(2), 205-224.

Wilding, B.V. and Beyer, K. (2017), “Force-displacement response of in-plane loaded unreinforced brick masonry walls: the critical diagonal crack model.” *B. Earthq. Eng*., Vol. **15**(5), 2201-2244.

Xiong, C., Lu, X., Lin, X., Xu, Z. and Ye, L. (2016), “Parameter determination and damage assessment for the-based regional seismic damage prediction of multi-story buildings.” *J. Earth. Eng*., Vol. **21**(3), 461-485.

Xie, L.L., Lu, X., Guan, H. and Lu, X.Z. (2015), “Experimental study and numerical model calibration for earthquake-induced collapse of RC frames with emphasis on key columns, joints, and the overall structure.” *J. Earth. Eng*., Vol. **19**(8): 1320-1344.

Yekrangnia, M., Bakhshi, A. and Ghannad, M.A. (2017), “Force-displacement model for solid confined masonry walls with shear-dominated failure mode.” *Earthq. Eng. Struct. Dyn*., Vol. **46**(13), 2209-2234.

Yu, L.L, Dong, Z.Q. and Li, G. (2022), “Simplified mechanical models for the seismic collapse performance prediction of unreinforced masonry structures.” *Eng. Struct*., Vol. **258**.

Zhai, C.H., Wen, W.P. Chen, Z. Li, S. and Xie, L.L. (2013), “Damage spectra for the mainshock-aftershock sequence-type ground motions.” *Soil Dyn. Earth. Eng.,* Vol. **45**, 1-12.